metals

Supplementary Material for "Enhanced Fatigue Resistance of Nanocrystalline $Ni_{50.8}Ti_{49.2}$ Wires by Mechanical Training"

Peng Chen [1,2], Xiaorong Cai [1,2,*], Na Min [3], Yunfan Liu [4], Zhengxiong Wang [1], Mingjiang Jin [1,*] and Xuejun Jin [1,2]

[1] Institute of Phase Transformation and Complex Microstructure, School of Materials Science and Engineering, Shanghai Jiao Tong University, Shanghai 200240, China
[2] Institute of Medical Robotics, Shanghai Jiao Tong University, Shanghai 200240, China
[3] Key Laboratory for Microstructures, Shanghai University, Shanghai 200444, China
[4] Institute of Forming Technology and Equipment, School of Materials Science and Engineering, Shanghai Jiao Tong University, Shanghai 200030, China
* Correspondence: cxr1110@sjtu.edu.cn (X.C.); jinmj@sjtu.edu.cn (M.J.)

1. Selection principle of training system

Under strain-controlled training procedure, the effective strain applied to the samples decreases as the residual strain accumulates, thereby weakening the training effect and prolonging the training period. However, upon stress-controlled training, the externally applied load is not affected by the accumulation of residual strain, making training more efficient and simpler. Figure S1 shows the macroscopic stress-strain curve of the NiTi wires used in this work upon stress-controlled loading with a peak stress of 700 MPa. It is seen that the martensitic transformation has not be completed when loaded to 500 MPa and the corresponding macroscopic strain is 5.2%. It is insufficient to train samples for the fatigue tests under the maximum strain of 5%. When loaded above 600 MPa, phase transformation is complete. At the same time, to avoid introducing too much plastic deformation during training, the peak stress of training is chosen to be 600 MPa. Thus, stress-controlled training with a peak stress for 60 cycles is chosen in this work.

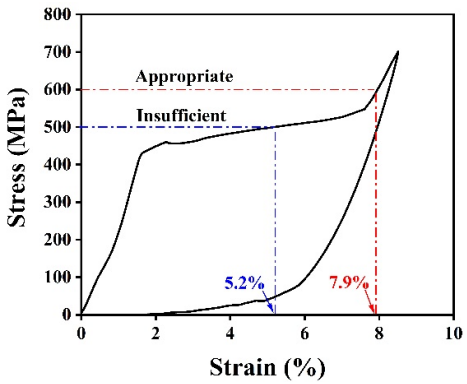

Figure S1. The loading-unloading stress-strain curve of uniaxial tension with a peak stress of 700 MPa.

2. Rotation angle calculation

The amount of grain rotation during training process is evaluated by the average rotation angle using the grain orientations extracted from TKD results. The orientation of each grain is defined by Bunge Euler angles $[\phi_1, \Phi, \phi_2]$, that represent rotations around $z - x' - z''$ axes, where $'$ indicates the newly rotated axis [1]. The grain orientations of the as-received sample and the trained sample, as are shown in Figure 7, are respectively listed in Table S1 and Table S2 using the Euler angles.

Table S1. The grain orientations extracted from the as-received sample. The Euler angles are in degrees.

Grain number	ϕ_1	Φ	ϕ_2
1	171.7°	31.71°	87.7°
2	173.07°	34.84°	85.96°
3	292.17°	40.14°	43.54°
4	336.11°	36.75°	46.37°
5	324.44°	36.87°	13.8°
6	348.31°	44.85°	24.57°
7	137.43°	18.73°	4.88°
8	349.33°	40.4°	20.03°
9	5.99°	30.2°	21.6°
10	322.34°	42.09°	23.8°
11	334.53°	45.05°	64.68°
12	324.67°	36.19°	12.59°
13	358.31°	28.59°	32.85°
14	233.82°	47.58°	65.92°
15	151.17°	36.94°	74.18°
16	27.26°	42.93°	15.72°
17	350.24°	36.14°	15.64°
18	26.82°	31.88°	22.05°
19	125.98°	33.26°	9.75°
20	349.48°	46.73°	23°
21	155.18°	34.94°	81.39°
22	324.8°	44.06°	15.62°
23	133.7°	19.53°	10.11°
24	171.87°	24.25°	67.24°

Table S2. The grain orientations extracted from the trained sample. The Euler angles are in degrees.

Grain number	ϕ_1	Φ	ϕ_2
1	59.62°	45.51°	78.59°
2	209.89°	37.9°	13.01°
3	76.75°	33.6°	34.37°
4	209.42°	31.46°	6.06°
5	332.51°	35.27°	88.15°
6	209.16°	40.89°	11.75°
7	49.95°	42.56°	71.48°
8	214.31°	40.76°	9.8°
9	205.69°	44.59°	13.08°
10	114.2°	33.82°	19.26°
11	211.49°	40.82°	5.72°
12	219.92°	44.16°	7.65°
13	48.53°	37.84°	76.69°
14	51.05°	42.82°	76.23°
15	331.37°	31.34°	5.47°
16	110.76°	34.59°	30.24°
17	67.59°	37.62°	45.73°
18	217.6°	41.53°	10.53°

The rotation is calculated as the lattice difference between the as-received grains and the trained grains. The rotation angle α is computed as follows [2]: 1. Choose grain A from the as-received sample and grain B from the trained sample and calculate their rotation matrices g_A and g_B based on the Euler angles. 2. The orientation relationship between grain A and grain B can be described as: $\Delta g = g_A g_B^{-1}$, where g_B^{-1} is the inverse of matrix g_B. 3. The rotation angle α between two orientations can be computed as $\cos\alpha = \frac{1}{2}(\Delta g_{ii} - 1)$. Note the crystal symmetry needs to be considered so the rotation angle α is the minimum rotation among all possible pairs of symmetrically equivalent orientations.

In this work, grain A is chosen from 24 grains listed in Table S1 and grain B is from 19 grains in Table S2. The rotation is calculated using the above method. The results show that the average rotation angle due to training process is 17°, rendering a strong <111> || DD texture.

3. Finite element simulation details

The geometry used for finite element simulations is established using a 3D finite element mesh generator Gmsh-3.0.3. The grain size and the microstructure are assigned according to the TKD results. The grain orientations of the as-received sample and the trained sample are respectively listed in Table S3 and Table S4 using the Euler angles.

Table S3. The grain orientations extracted from the as-received sample. The Euler angles are in degrees.

Grain number	ϕ_1	Φ	ϕ_2
1	348.31°	51.85°	24.57°
2	1.75°	60.14°	44.17°
3	292.17°	40.14°	43.54°
4	324.8°	44.06°	15.62°
5	349.33°	40.47°	20.03°
6	350.24°	36.14°	15.64°
7	337.11°	44.75°	320.37°

Table S4. The grain orientations extracted from the trained sample. The Euler angles are in degrees.

Grain number	ϕ_1	Φ	ϕ_2
1	359.17°	57.6°	43.89°
2	309.89°	51.1°	45.01°
3	356.75°	50.36°	46.57°
4	349.42°	54.46°	46.96°
5	331.37°	67.34°	5.47°
6	337.16°	55.89°	48.75°
7	349.95°	59.36°	43.28°

The elastic constants and the mechanical properties used in the simulation are listed in the Table S5. The critical stresses to trigger phase transformation are 426 MPa and 333 MPa for the as-received and the trained sample, respectively.

Table S5. The elastic constants and the mechanical properties used in the simulation (all units are in GPa except for υ) [3]

c_{11}	c_{12}	c_{44}	E	G	υ
175	145	35	71	25	0.42

The simulations are performed using a finite element multiphysics object-oriented simulation environment (MOOSE) using the model presented in reference [4–6]. The contour plots shown in Figure 12 are strain components and strain energy density calculated when the applied strain is 5%.

4. XRD results

Figure S2 shows the intensity normalized XRD results based on the $(110)_{B2}$, and the as-received sample was composed of cubic austenite (B2) and little R phase. No residual martensite was detected for the trained samples.

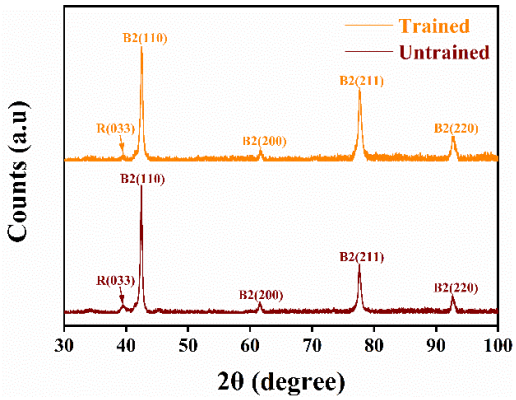

Figure S2. X-ray diffraction profiles of the NiTi shape memory alloy wires.

References

1. Cai, X.; Handwerker, C.A.; Blendell, J.E.; Koslowski, M. Shallow grain formation in Sn thin films. *Acta Mater.* **2020**, *192*, 1–10, https://doi.org/10.1016/j.actamat.2020.03.014.
2. Jahedi, M.; Ardeljan, M.; Beyerlein, I.J.; Paydar, M.H.; Knezevic, M. Enhancement of orientation gradients during simple shear deformation by application of simple compression. *J. Appl. Phys.* **2015**, *117*, 214309, https://doi.org/10.1063/1.4922032.
3. Wagner, M.F.-X.; Windl, W. Elastic anisotropy of Ni4Ti3 from first principles. *Scr. Mater.* **2009**, *60*, 207–210, https://doi.org/10.1016/j.scriptamat.2008.09.028.
4. B. Alger, D. Andrš, R.W. Carlsen, D.R. Gaston, F. Kong, A.D, Lindsay, J.M. Miller, C.J. Permann, J.W. Peterson, A.E. Slaughter, R. Stogner, MOOSE Web page, 2020. https:// moose frame work.org, accessed on 2 August 2021.
5. J.C. Simo, T.J.R. Hughes, Computational Inelasticity: Volume 7 of Interdisciplinary Applied Mathematics, Springer-Verlag, Secaucus, USA, 1998.
6. Xu, L.; Solomou, A.; Baxevanis, T.; Lagoudas, D. Finite strain constitutive modeling for shape memory alloys considering transformation-induced plasticity and two-way shape memory effect. *Int. J. Solids Struct.* **2020**, *221*, 42–59, https://doi.org/10.1016/j.ijsolstr.2020.03.009.